

Fiber reinforced concrete L-beams under combined loading

Omer Farouk Ibraheem^{*}, B.H. Abu Bakar^a and I. Johari^b

Department of Civil Engineering, University Sains Malaysia (USM), Penang, Malaysia

(Received September 20, 2013, Revised May 2, 2014, Accepted May 2, 2014)

Abstract. The addition of steel fibers in concrete mixture is recognized as a non-conventional mass reinforcement scheme that improves the torsional, flexural, and shear behavior of structural members. However, the analysis of fiber reinforced concrete beams under combined torsion, bending, and shear is limited because of the complicated nature of the problem. Therefore, nonlinear 3D finite element analysis was conducted using the “ANSYS CivilFEM” program to investigate the behavior of fiber reinforced concrete L-beams. These beams were tested at different reinforcement schemes and loading conditions. The reinforcement case parameters were set as follows: reinforced with longitudinal reinforcement only and reinforced with steel bars and stirrups. All beams were tested under two different combined loading conditions, namely, torsion-to-shear ratio (T/V) = 545 mm (high eccentricity) and T/V = 145 mm (low eccentricity). Eight intermediate L-beams were constructed and tested in a laboratory under combined torsion, bending, and shear to validate the finite element model. Comparisons with the experimental data reveal that the program can accurately predict the behavior of L-beams under different reinforcement cases and combined loading ratios. The ANSYS model accurately predicted the loads and deformations for various types of reinforcements in L-beams and captured the concrete strains of these beams.

Keywords: L-beam; fiber-reinforced concrete; combined loading; finite element analysis

1. Introduction

The existing methods for analyzing beams under torsional forces can be broadly classified into two main categories, namely, analytical models and numerical methods, such as finite element models. Torsion theories have been developed by numerous researchers, and good results have been achieved through the effective description of the behavior of these members. These models can be divided into two main theories, namely, Skew-Bending theory, which was the basis of the American code between 1977 and 1995, and Space Truss Analogy, which is the current basis of the American code (since 1995) and the European model code (since 1978) (Bernardo and Lopes 2008).

These theories are only applicable to normal concrete. A number of researchers have extended these theories to explain the analytical response of fiber reinforced concrete elements. Karayannis

^{*}Corresponding author, Ph.D. student, E-mail: omerfarouk77@yahoo.com

^aProfessor, Ph.D. E-mail: cebad@eng.usm.my

^bPh.D.

(2000) predicted the full torsional behavior of steel fiber-reinforced concrete (SFRC) members without reinforcing bars. The model was efficient and used for rectangular and flanged members under pure torsion. Softened truss model theory (Hsu and Mo 1985) has been modified to include the influence of steel fibers and has successfully been applied in fiber reinforced concrete rectangular beams with steel bars and stirrups (Mansur *et al.* 1989, Gunneswara Rao and Rama Seshu 2005). Ju *et al.* (2013) employed the modified fixed angle softened truss model (Hsu and Zhang 1997) to estimate the torsional behavior of SFRC rectangular members under pure torsion. The analytical model provided an excellent estimation of the overall torsional behavior and strength.

Simplified semi-empirical expressions and formulas for code modification have been proposed to calculate the ultimate torsional capacity of fiber reinforced concrete beams with rectangular cross-section (Mansur and Paramasivam 1985, Craig *et al.* 1986, Wafa *et al.* 1992, Gunneswara Rao and Rama Seshu 2003); good results have been obtained for rectangular beams without steel reinforcement.

A greater number of studies on fiber reinforced concrete rectangular beam behavior under combined loading can be found in the literature (Avinash 2010, Mansur and Paramasivam 1985) compared with those in the field of pure torsion. These studies were concerned with beams with rectangular sections that were not reinforced by steel bars (Mansur and Paramasivam 1985) or those that were reinforced with longitudinal and transverse reinforcements (Avinash 2010). Meanwhile, the research on flanged fiber reinforced concrete beams under combined loading remains limited.

Finite element analysis have focused mainly on plain concrete beams (without fibers) with rectangular cross-section under pure torsion (Bhatti and Almughrabi 1996, Mahmood 2007) or under combined torsion and bending (Santhakumar *et al.* 2007). Finite element analysis on fiber reinforced concrete beams under combined loading remains inadequately explored.

L-beams located at the perimeters of buildings bear loads from slabs, joists, and beams from only one side of the member. This loading mechanism generates torsional forces that are transferred from the spandrel beams to the columns. These beams are not only influenced by torsional loads; other loads that accompany torsional loads include bending and shear loads. The end beams with slabs on only one side have a typical L-shape, from which the name “L-beam” was derived (Wight and Macgregor 2009). The aforementioned loads, along with the non-symmetric shape, cause this type of beam to be influenced by a complex combination of stresses; such complexity prevents the extensive study of this subject.

In this study, a finite element program called ANSYS CivilFEM was used to analyze the behavior of fiber-reinforced concrete L-beams under combined torsion–bending–shear loading at different values of eccentricities, T/V, and steel reinforcement cases.

Eight L-shaped beams were cast and tested in a laboratory under different steel reinforcement cases to validate the finite element model developed in this study.

2. Experimental program

The experimental program included 8 L-shaped spandrel beams tested under combined torsion, bending, and shear, and sorted into two groups based on conventional steel reinforcements. Tested beams were constructed using steel fiber concrete with 1.0% and 1.5% volume fractions of fibers.

2.1 Materials

The concrete mix consisted of ordinary Portland cement manufactured locally, river sand with a fineness modulus of 2.6, and coarse aggregate with a maximum size of 19.5 mm.

The concrete mixture was made using cement, sand, and crushed aggregate with a mixture proportion of 1:2:2.5 and water cement ratio of 48%. The mixture was designed to have a specified 28-day strength of 40.0 MPa.

The prepared fresh fiber reinforced concrete mixture was carefully placed in molds for the specimens and vibrated for a sufficient period by a portable electrical vibrator to ensure suitable consolidation of the mixture. Concrete test cubes and cylinders were cast simultaneously with the test beams for each mixture and vibrated using a frequency-vibrating table. The average concrete strength values of the tested beams are presented in Table 1. The code names of the tested beams comprise three parts. The first part represents the beam reinforcement case: longitudinal



Fig. 1 Hooked-end steel fibers

Table 1 Material properties of the tested beams

Group No.	Beam name	Volume of steel fiber (%)	Compressive strength at 28 days (MPa)	Split tensile strength at 28 days (MPa)
I	L1-145	1.0	43.0	5.7
I	L1.5-145	1.5	46.0	5.9
I	L1-545	1.0	46.0	6.3
I	L1.5-545	1.5	42.2	7.1
II	S1-145	1.0	44.0	5.5
II	S1.5-145	1.5	41.4	6.1
II	S1-545	1.0	41.0	5.0
II	S1.5-545	1.5	35.5	6.0

reinforcement only (L), and longitudinal and stirrups (S). The second part represents the steel fiber volume ratio: 1% and 1.5%. The third part represents the load eccentricities, that is, 545 mm and 145 mm.

Bent-ended steel fibers, as shown in Fig. 1, with aspect ratios $l_f/d_f = 60/0.75 = 80$ were used, where l_f denotes fiber length and d_f denotes fiber diameter. Two steel fiber volume fractions, V_f , were adopted, namely: (1) a moderate one equal to 1% or 78.5 kg per 1 m³ concrete and (2) a ratio limited by practical considerations in structural members equal to 1.5% or 117.75 kg per 1 m³ concrete (Wight and Macgregor 2009). The average yield strength of the steel fibers provided by the manufacturer was $f_{yf} = 1100$ MPa (± 100 MPa).

The average yield strength of the steel reinforcement was 420, 570 and 450 MPa for a diameter of 12, 10, and 6 mm, respectively.

2.2 Tested beams

Eight identical reinforced concrete spandrel beams were manufactured according to the design guidelines outlined in ACI 318 (2005). The beams were 2500 mm long with an L-shaped cross section. The 100 mm \times 150 mm flange represented a section of the floor slab at the perimeter of an reinforced concrete diaphragm. Tested beams were sorted into two groups based on their conventional steel reinforcement. The first group included four beams with longitudinal reinforcement only, and the second group included beams with longitudinal reinforcement and stirrups.

The beams of the first group were reinforced with longitudinal bars ($2\phi 12$ mm) at the bottom and ($3\phi 10$ mm) at the top. The beams of the second group had the same longitudinal reinforcement details as group one beams with the addition of stirrups ($\phi 6$ mm/100 mm). All beams were over-reinforced at the ends and at mid span to avoid concrete crushing because of stress concentration. Fig. 2 displays the details of the tested beam specimens.

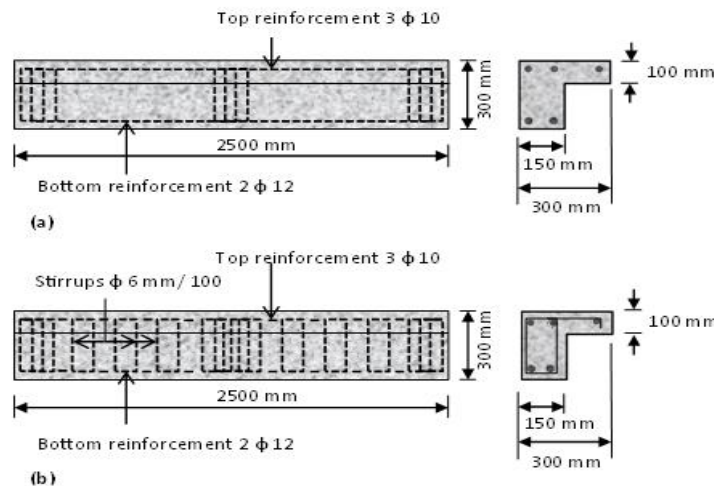


Fig. 2 Elevation, cross-sectional dimensions, and steel reinforcement details of the tested beams: (a) Group I, (b) Group II

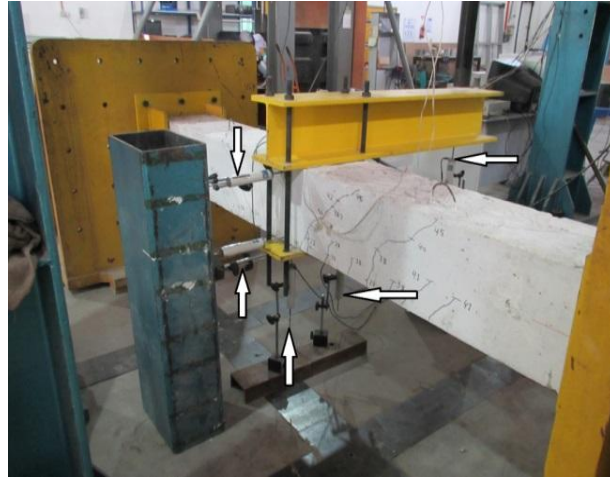


Fig. 3 Test rig and LVDT distribution

2.3 Test setup

The specimens were allowed to rest at the ends on L-shaped steel supports over a constant span of 2200 mm. The supports did not permit horizontal movement, vertical movement, and rotation around the beam axis. At mid span, a lever arm of an I-section steel beam was attached to the top face of the beam and tightly bolted around the spandrel beam (Fig. 3). A hydraulic compressor with a 450 kN capacity was applied on the lever arm at any eccentricity (e) to achieve the required torque-to-shear (eccentricity) ratio. The load was imposed at a constant load step and measured by a load cell with an accuracy equal to 0.05 kN. The average angle of twist and vertical displacement at mid span of the tested beams were measured using the measurements of a set of linear variable displacement transducers (LVDT) with an accuracy of 0.02 mm placed along the steel arm and backside of the beam, as shown in Fig. 3. To capture each significant detail of the behavior of the specimens, constant loading rate were selected for each group.

3. Finite element modeling

3.1 Element types

Reinforced concrete is a composite material made of two materials with different physical and mechanical behavior, namely, concrete and steel. The behavior of RC is nonlinear because of the nonlinear behavior of concrete with reinforced steel. Concrete and reinforcing steel are represented by separate material models, which are combined to characterize the behavior of the composite RC material.

Concrete was modeled by using a 3D structural RC solid element, SOLID65. The reinforcement was modeled by using 3D spar element, Link8. The 3D structural solid element SOLID45 was used to model the structural steel (ANSYS 2012).

3.2 Material properties

3.2.1 Concrete

A library of the ANSYS CivilFEM program has provided the stress-strain diagram for the structural analysis of concrete. PCA parabolic type stress–strain curve, as shown in Fig. 4, was used to model concrete in compression. The model can incorporate the softening of concrete

For tension, the stress-strain curve for concrete is linearly elastic approximately up to the maximum tensile strength. After this point, the concrete cracks and the strength gradually decreases to zero (Bangash 1989). The effect of stiffening tension under the cracked tensile condition is incorporated by using the stiffness multiplier constant (T_c). After cracking, the uniaxial tensile strength of the concrete (f_t) drops abruptly to a fraction of it ($T_c f_t$) and approaches zero at a strain that is six times the cracking strain, as shown in Fig. 5. The authors have performed a parametric study by varying the value of T_c . The results remain unchanged. Therefore, a default value of 0.6 was used for all analyses and was incorporated in ANSYS CivilFEM.

Thus, the FE input data for concrete material required by ANSYS CivilFEM are as follows:

- Concrete age;
- Ultimate uniaxial compressive strength (f_c);
- Ultimate uniaxial tensile strength (f_t);
- Shear transfer coefficient (β_t);
- Stiffness multiplier constant (T_c).

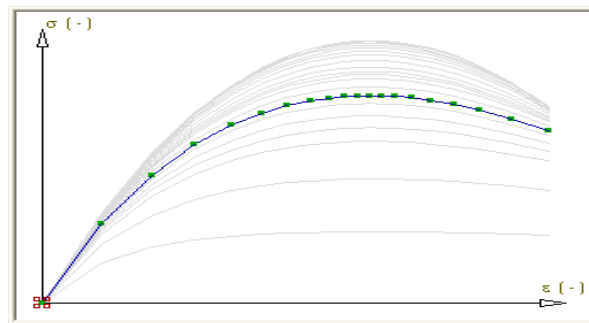


Fig. 4 Concrete stress-strain model in compression (ANSYS CivilFEM 2012)

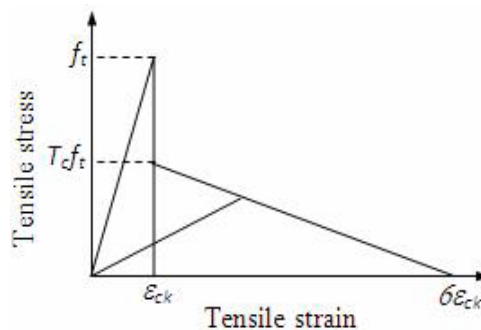


Fig. 5 Stress–strain model for concrete in tension(ANSYS 2012)

The shear transfer coefficient βt represents the conditions of the crack face. The value of βt ranges from 0.0 to 1.0, with 0.0 representing a smooth crack (complete loss of shear transfer) and 1.0 representing a rough crack (without any loss of shear transfer) (ANSYS 2012). However, the value of βt used in numerous studies on RC structures varies between 0.05 and 0.25 (Bangash 1989; Huyse *et al.* 1994). A number of preliminary analyses were attempted by using various values of βt within this range to avoid convergence problems (Kachlakev *et al.* 2001, Santhakumar 2007). In the present study, the shear transfer coefficient of 0.2 for an open crack was found to be suitable for analyzing the beams subjected to combined bending, torsion and shear. A higher value of 0.22 was used as βt for a closed crack.

3.2.2 Steel reinforcement and structural steel

The steel reinforcement used for the FE models is always assumed to be a perfectly elastic, plastic material that is identical in tension and compression.

A bilinear stress-strain curve was provided by the ANSYS CivilFEM program to model the reinforcing and structural steel under tension and compression, as shown in Fig. 6.

The steel reinforcement is incorporated into the concrete by using the discrete model, embedded model, or smeared model, depending on the geometry of the system. First, in the discrete model, spar or beam elements with geometrical properties similar to the original reinforcing elements are connected to concrete mesh nodes. Thus, the concrete and reinforcement mesh share the same nodes. The concrete mesh is restricted by the location of the reinforcement. Furthermore, the concrete occupies the same regions occupied by the reinforcement. The volume of the steel reinforcement is not deducted from the concrete volume (Kachlakev *et al.* 2001).

Second, the embedded model overcomes the concrete mesh restriction because the stiffness of the reinforcing steel is separately evaluated from the concrete elements. The model is built in a way that maintains the reinforcement of steel displacements that are compatible with the surrounding concrete elements. This model is advantageous for complex reinforcement details. However, this model increases the number of nodes and degrees of freedom, which in turn increase the run time and computational cost.

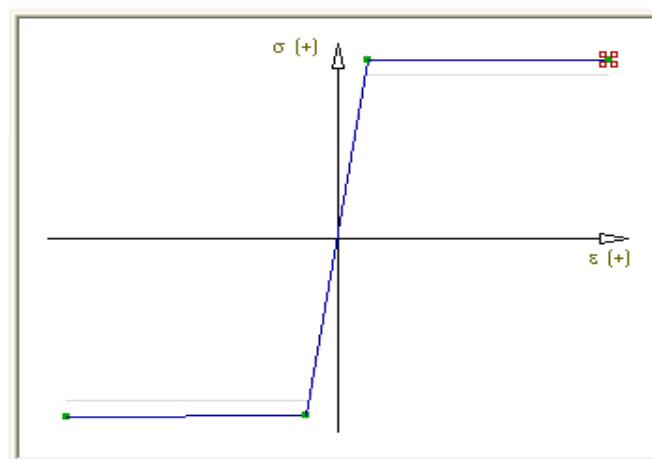


Fig. 6 Stress–strain curve for reinforcement and structural steel (ANSYS CivilFEM 2012)

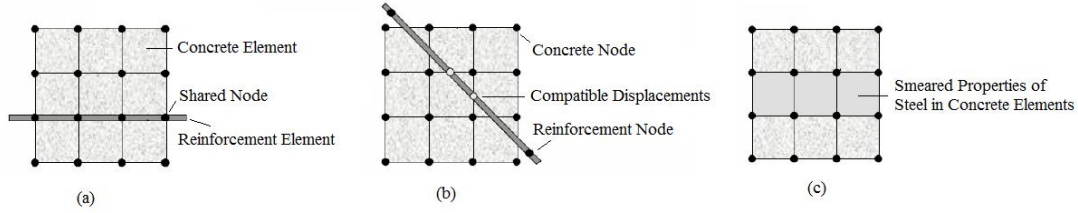


Fig. 7 Models for reinforcement in reinforced concrete (Tavarez 2001): (a) discrete, (b) embedded, and (c) smeared

Third, the smeared model assumes that the reinforcement is uniformly spread throughout the concrete elements in a defined region of the FE mesh. The effect of reinforcement is averaged within the pertaining concrete element (Dahmani *et al.* 2010). The features of the above techniques are schematically shown in Fig. 7. Therefore, the discrete modeling approach provides an accurate and true representation of reality for modeling of RC beams with well-defined geometry and reinforcement details. Earlier researchers (Kachlakev *et al.* 2001; and Dahmani *et al.*, 2010) also suggested the discrete modeling strategy because of the facts stated above. Thus, in this study, discrete modeling was followed by the modeling of longitudinal and transverse steel bars.

3.2.3 Steel fibers

The effectiveness of steel fibers in increasing the tensile strength of the concrete depends on the number of fibers per unit cross-sectional area of concrete.

Padmarajaiah and Ramaswamy (2002) and Thomas and Ramaswamy (2006) calculated the number of fibers per unit area along the beam length according to the probability approach given by Parviz and Lee (1990). Thus, the number of fibers per unit cross-sectional area of concrete can be calculated (Parviz and Lee 1990) by:

$$N_f = \eta_0 \left(\frac{4V_f}{\pi d_f^2} \right) \quad (1)$$

where

N_f : number of fibers per unit cross section area;

V_f : Volume fraction of steel fibers;

d_f : diameter of steel fiber;

η_0 : the orientation factor ranging from 0.41 to 0.82 (Swamy and Al-ta'an 1981; Parviz and Lee 1990).

In their study, the fibers have been modeled discretely by using the element Link8, as shown in Fig. 7a. The area of the Link8 element representing the fiber has been computed by:

$$A_f = \eta_0 V_f A_e \quad (2)$$

where A_e is the cross-sectional area of a concrete element.

This modeling approach presents the rectangular and flanged beams under flexural loads having good agreement with experimental data (Padmarajaiah and Ramaswamy 2002, Thomas and

Ramaswamy 2006). In the present study, the idealization as smeared concrete element will be used to model the steel fibers in the concrete. In this case, the concrete and reinforcement were discretized into elements with the same geometrical boundaries. The effects of reinforcement were averaged within the element (Fig. 7c). This method appears to be more rational compared with the discrete model when modeling the steel fibers within the concrete element.

The nonlinear material behavior of the fibers was input into the ANSYS CivilFEM program as an independent, material, nonlinear stress-strain curve. A bilinear stress-strain curve provided by the program to model reinforcing and structural steel was employed to model the stress-strain curve of steel fibers (Fig. 6).

3.3 Element properties

The individual elements contain different properties. The element SOLID65 requires properties for rebar, assuming a smeared model. These values include material number, volume ratio, and orientation angles. In this study, the beams are modeled by using the discrete reinforcement technique. Therefore, for all properties, a value of zero was entered, which turned the smeared reinforcement capability of the element SOLID65 off, except in cases of the representation of steel fibers as a smeared layer.

Element properties are needed to define the element Link8. Thus, the values for the cross-sectional area and initial strain were entered for all steel bars. A value of zero was entered for the initial strain because no initial stress is found in the reinforcement. No element properties set exist for the element SOLID45.

3.4 Beam modeling

Half of the full beam was used for modeling by maximizing the symmetry of the beam. This approach significantly reduced computational time and computer disk space requirements. The beam, steel arm, and supports were modeled as volumes. Given that a half of the beam is being modeled, the model is 1250 mm long with a cross-section measuring 150 mm wide and 300 mm

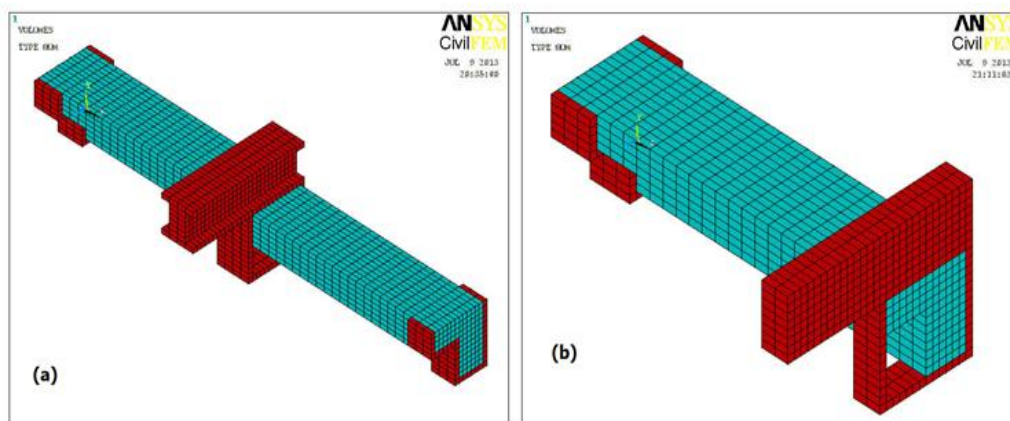


Fig. 8 Spandrel beam volumes: (a) full size (b) half size

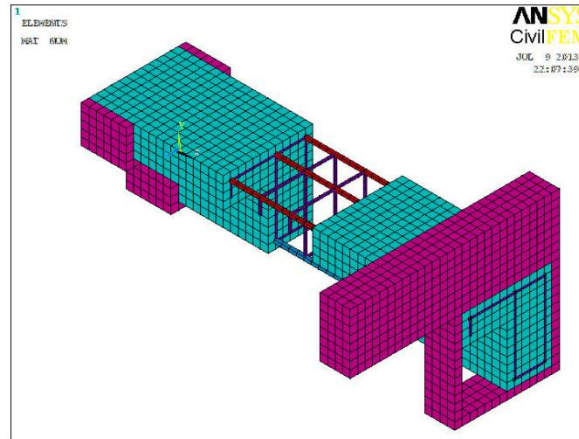


Fig. 9 Spandrel beam mesh

high (web), and 300 mm wide and 100 mm thick (flange). The origin point for the X , Y , and Z coordinates coincides with the lower corner of the web. The volume of the full and half sizes of the entire model are shown in Fig. 8.

3.5 Meshing

Concrete was modeled by using the element SOLID65 (nonlinear RC element). The most important aspect of Solid65 element is the treatment of nonlinear material properties and capable of cracking under tension and crushing under compression. Using a rectangular mesh is recommended to obtain good results from SOLID65. Therefore, the mesh was set up such that square elements were created with a dimension of 25 mm in all three directions.

In the FE models, 3D spar elements, Link8, were employed to represent longitudinal and transverse steel reinforcement, referred to here as link elements. While SOLID45 element was used to model the steel supports and steel loading arm.

The width and length of the elements in the support and loading arm were defined properly to be consistent with the elements and nodes in the concrete portions of the model. Fig. 9 shows the overall mesh of the concrete, steel reinforcement, support, and arm.

3.6 Boundary conditions and loading

The displacement boundary conditions are required to constrain the model to obtain a unique solution. To ensure that the model performs the same way as the experimental beam, boundary conditions need to be applied at points of symmetry, as well as where the supports and loadings exist. First, the symmetry boundary conditions were set. The model used is symmetric in one plane.

The nodes defining a plane through the beam mid-span define a plane of symmetry. To build a model of the symmetry, the nodes on this plane must be constrained in the horizontal direction. Therefore, these nodes have a degree of freedom constraint at $UX = 0$.

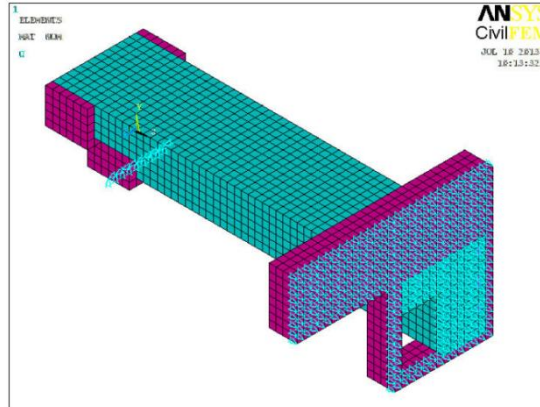


Fig. 10 Boundary condition for the plane of symmetry and support condition

The support was modeled in such a way that a roller was created. A singular line of nodes on the support were provided with a constraint in the UY and UZ directions, applied as constant values of 0. As such, the beam will be allowed to rotate at the support. The boundary conditions for the plane of symmetry and the support condition are shown in Fig. 10.

3.7 Load stepping and failure definition

In this study, the total load applied was divided into a series of load steps. Newton–Raphson equilibrium iterations provide convergence at the end of each load increment within tolerance limits. The automatic time stepping in the ANSYS CivilFEM program predicts and controls load step sizes, which require maximum and minimum load step sizes. After several attempts, the number of load steps, that is, the minimum and maximum step sizes, was determined. The loads were applied gradually with smaller load increments during concrete cracking, steel yielding, and ultimate stage, in which numerous cracks occur. Beam failure occurs when convergence fails with small load increment.

4. Results and discussion

This section presents the results of the ANSYS CivilFEM and compares them with the experimental data for the steel fiber reinforced concrete L-shape beams tested under combined loading. The following comparisons contain torque-twist plots, load-deflection plots and load-concrete strain plot.

4.1 Torque-twist plot

Figs. 11 and 12 compare the torque-twist plots for beams L1-545 and L1.5-545, respectively. The torque-twist plot from the FE model conforms with the experimental data. The first cracking torque level for beam L1-545 on the basis of FE analysis is 4.4 kN.m, and the actual value is 6.0 kN.m; hence, a 26.67% difference. A beam failed in the model at 12.56 kN.m, with 2.4%

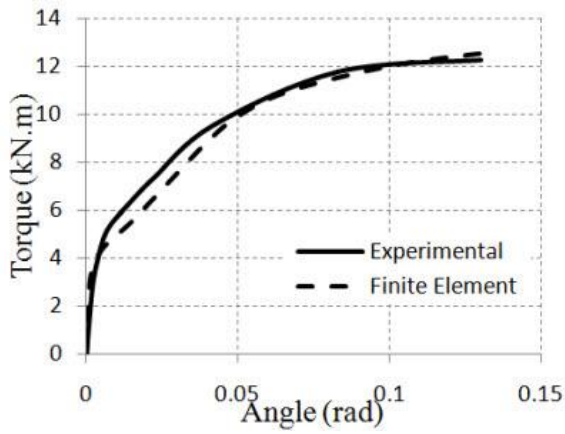


Fig. 11 Torque–twist curve for beam L1-545

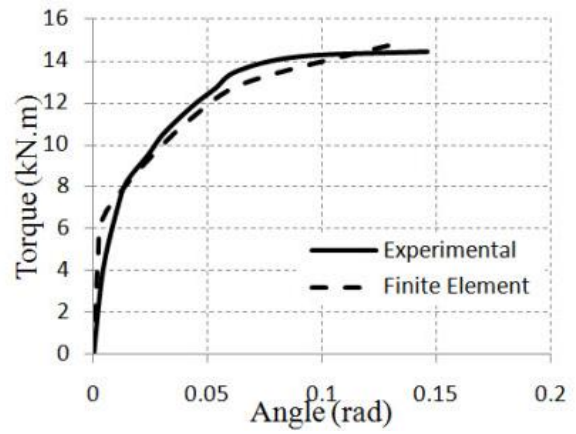


Fig. 12 Torque–twist curve for beam L1.5-545

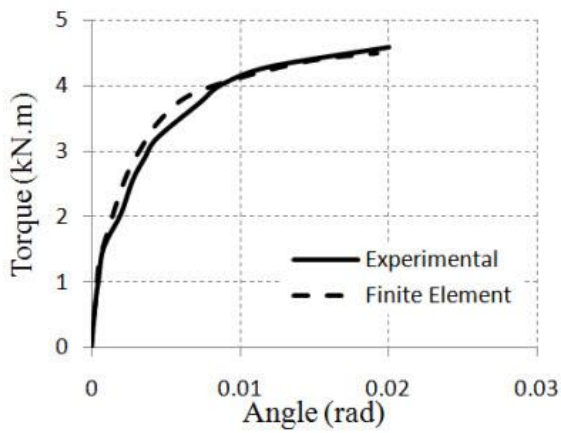


Fig. 13 Torque–twist curve for beam L1-145

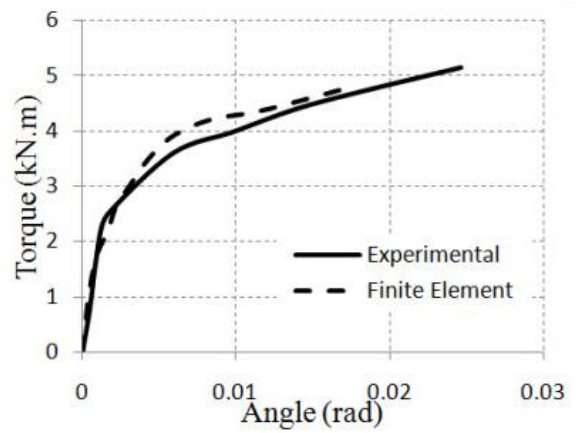


Fig. 14 Torque–twist curve for beam L1.5-145

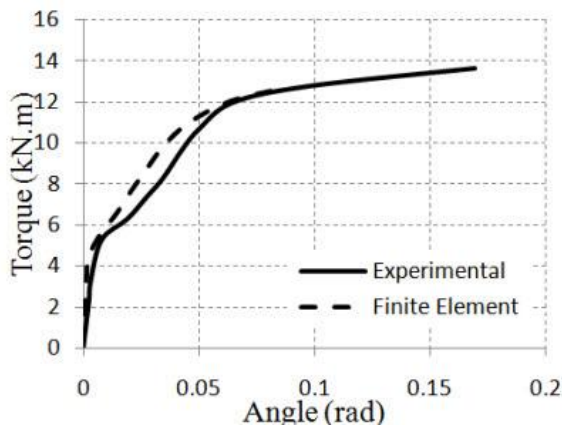


Fig. 15 Torque–twist curve for beam S1-545

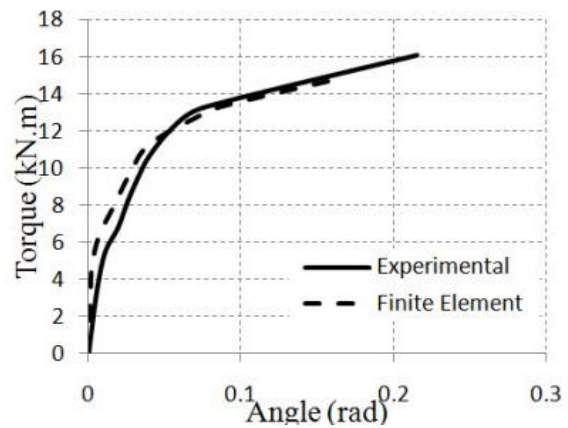


Fig. 16 Torque–twist curve for beam S1.5-545

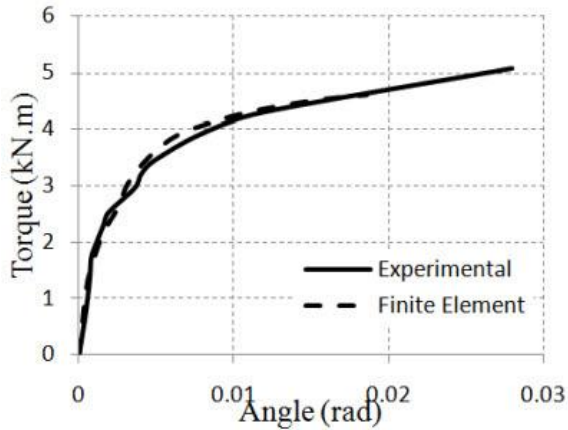


Fig. 17 Torque–twist curve for beam S1-145

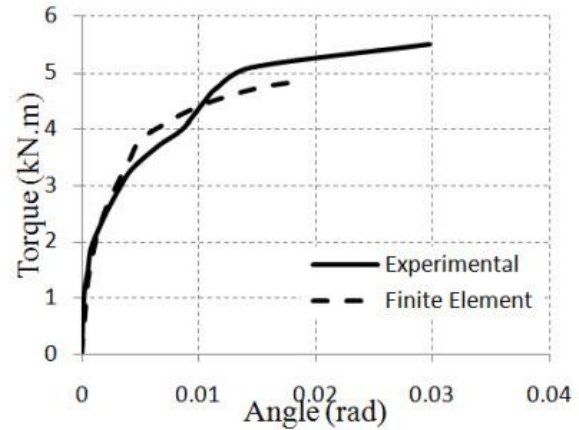


Fig. 18 Torque–twist curve for beam S1.5-145

difference with the experimental data.

The FE model for beam L1.5-545 cracks at 7.1 kN.m, which is 13.2% less than the actual beam torque level of 8.18 kN.m. The model and the actual beam failed at torques 14.7 and 14.44 kN.m, respectively, with 1.8% increase.

The model describes well the behavior of the two beams. Beam L1-545 slightly increases its stiffness prior to the crack and decreases its stiffness before beam failure. Beam L1.5-545 is stiffer than the actual data at elastic range. However, after cracking, the behavior overturned almost to the final load.

Beams L1-145 and L1.5-145 traced their torque-twist behavior by FE model, as presented in Figs.13 and 14. A 25.5% difference between the model and the actual data for the cracking torque level of beam L1-145 was noted in 1.4 kN.m of the model and 1.88 kN.m for the beam. Beam L1-145 failed at 4.6 kN.m and the FE model at 4.5 kN.m.

Beam L1.5-145 cracked at 2.18 kN.m and the model at 2.1 kN.m, which is a 3.7% difference. The beam failed at a torque level of 5.15 kN.m and the model at 4.8 kN.m, which is a 6.7% difference.

The FE model showed a stiffer behavior after the concrete crack of beam L1-145. This divergence disappears almost at the maximum load. The same behavior can be noted in beam L1.5-145, with a slight decrease in ductility before failure.

Figs.15 and 16 show that the FE model is stiffer than that of the actual beam for beams S1-545 and S1.5-545, respectively. The first beam cracked at 5.18 kN.m torque level and the FE model at 5.4 kN.m. When stirrups yield, the stiffness coincides with the actual values until the load fails. The model fails at 12.7 kN.m, and the beam at 13.63 kN.m.

FE analysis shows that the second beam cracks at 7.4 kN.m, which is 9% higher than the actual cracking torque. Stiffness reduced after the stirrups yielded, and the model failed at 14.9 kN.m, whereas the actual beam at 16.1 kN.m.

The plot for the torque-twist curves of beams S1-145 and S1.5-145 is illustrated in Fig. 17 and 18, respectively. The model cracked at 2.1 kN.m load level, with a 25.7% increase compared with the experimental result. The experimental data and the decrease in ductility match. The model fails at 4.6 kN.m, and the actual beam at 5.08 kN.m.

Beam S1.5-145 cracks at 2.03 kN.m and the FE model at 2.0 kN.m. Divergence is clear before and after the stirrups yield. Finally, at the torque level, the model fails at 4.8 kN.m, which is approximately 12% lower than the actual value. Compared with the experimental results, the model shows smaller torsional ductility.

4.2 Load-deflection plot

The load–deflection curves for the FE model and the actual experiment data for the specimens tested under higher bending moment will be reviewed here.

The FE analysis and the experimental data in Figs. 19 and 20 for beams L1-145 and L1.5-145, respectively, indicate good agreement and the FE analysis closely conforms with the experimental data for beams. After the longitudinal steel bars yield, the stiffness slightly decreases for the model

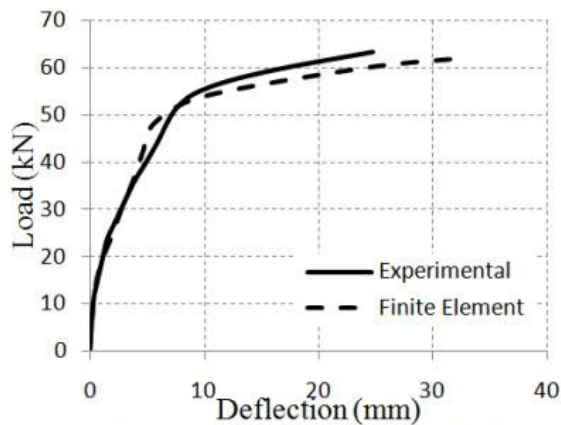


Fig. 19 Load–deflection curve for beam L1-145.

Fig. 19 Load–deflection curve for beam L1-145

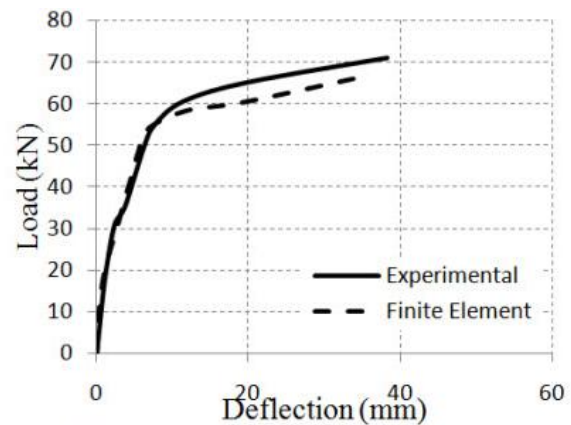


Fig. 20 Load–deflection curve for beam L1.5-145.

Fig. 20 Load–deflection curve for beam L1.5-145

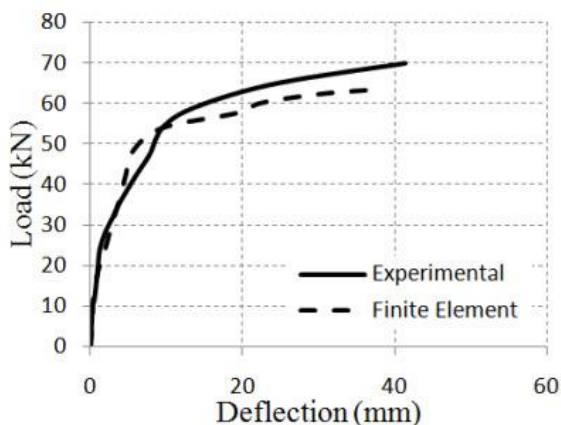


Fig. 21 Load–deflection curve for beam S1-145

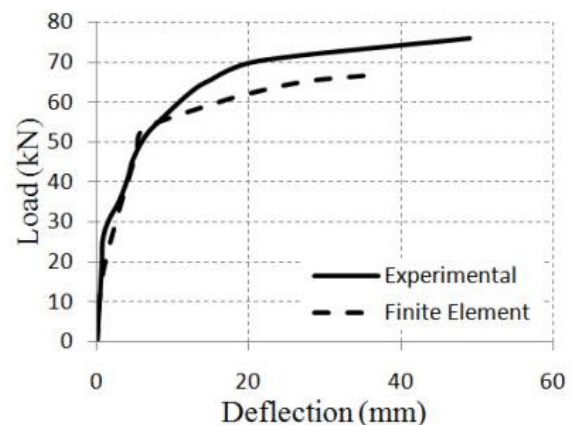


Fig. 22 Load–deflection curve for beam S1.5-145

before the final load; a divergence between data is observed almost near the maximum load.

Beams S1-145 and S1.5-145 behave almost similarly with beams S1-545 and S1.5-545. The difference is the disagreement between the experimental and the FE model after the steel reinforcement yields until the final load (Figs. 21 and 22).

The FE model in this study provides a perfect fit with the experimental data for the beams reinforced with steel fiber. Several factors may have caused the disagreement between the experimental data and the FE model. A perfect bond between the concrete and the steel reinforcement is assumed in the FE analyses. A uniform shear transfer coefficient for open and closed cracks in the concrete was assumed in the FE model, which may considerably affect model behavior. The orientation factor value for the steel fibers used in model. The number of elements used to model the beams. All these factors significantly affected the accuracy of the behavior (Kachlakev *et al.* 2001).

However, the smeared model for the steel fibers provides efficient results in the FE analysis of the fiber RC beams under combined loading.

4.3 Strain in concrete surface

The horizontal strain developed in the concrete beam was measured on the backside of the beam (away from the flange). A 20 mm strain gauge was placed at the mid-depth of the beam on the mid-span section.

Beam L1-545 was obtained when the specimens with longitudinal reinforcement with added 1.0% steel fibers were tested under high torsion ($e = 0.545$ m). The horizontal strains on the concrete surface of the beam were efficiently traced by the FE model, specifically with low stiffness after the concrete cracks to maximum load (Fig. 23).

The behavior of beam L1-545 is similar to that of beam L1.5-545 after the steel volume ratio was increased to 1.5%. The strain value and curve ductility increased compared with that of beam L1-545 (see Fig. 24).

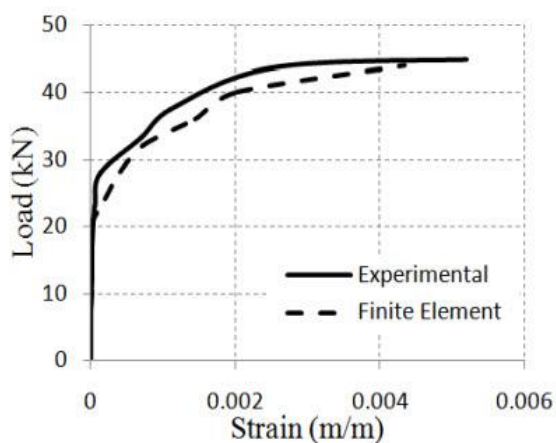


Fig. 23 Load-concrete strain curve for beam L1-545

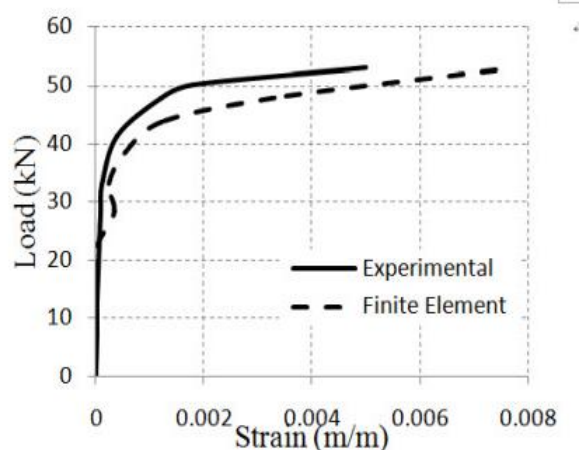


Fig. 24 Load-concrete strain curve for beam L1.5-545

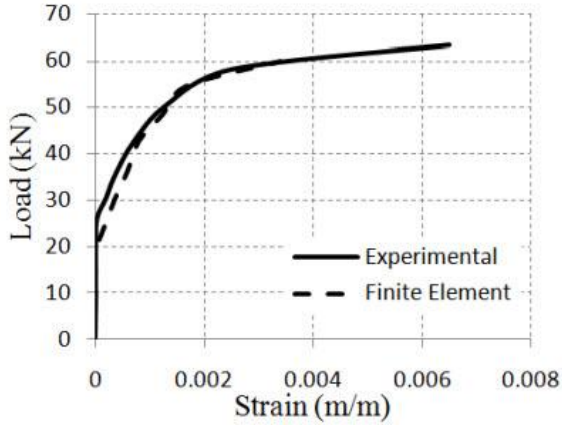


Fig. 25 Load-concrete strain curve for beam L1-145

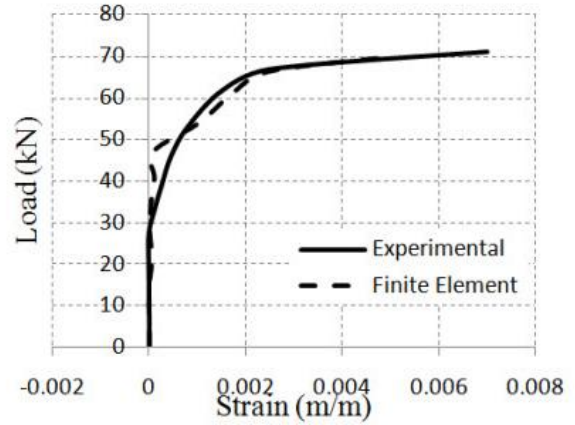


Fig. 26 Load-concrete strain curve for beam L1.5-145

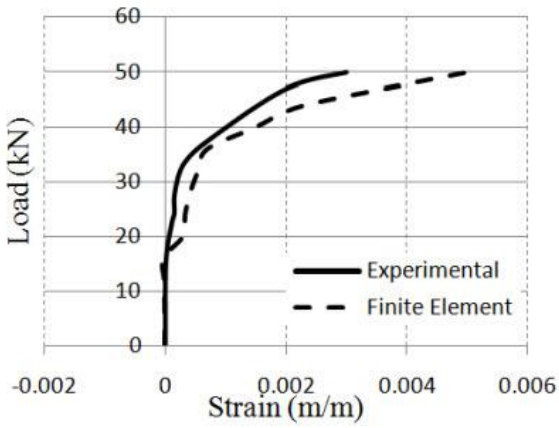


Fig. 27 Load-concrete strain curve for beam S1-545

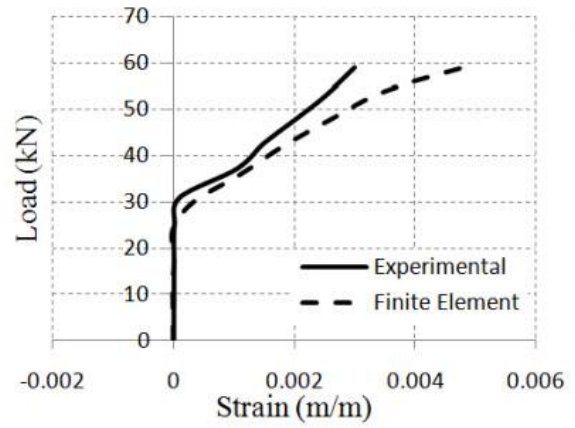


Fig. 28 Load-concrete strain curve for beam S1.5-545

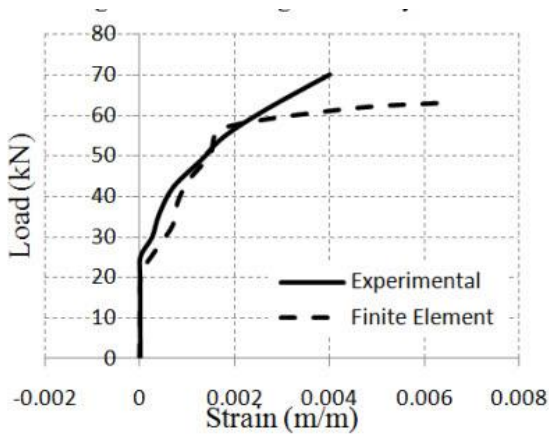


Fig. 29 Load-concrete strain curve for beam S1-145

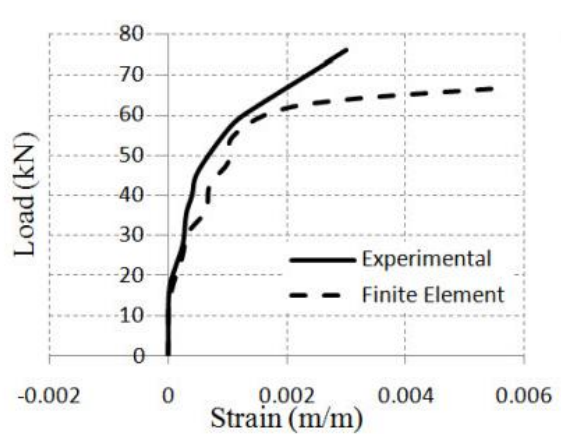


Fig. 30 Load-concrete strain curve for beam S1.5-145

Fig. 25 show that the model has good agreement with the behavior of beam L1-145 for strain cases under low eccentricity ($e = 0.145$).

The experimental and FE analyses indicate good agreement for the strain of beam L1.5-145 (Fig. 26). The disagreement between the experimental and model curves for the strain values is caused by the cracks in the maximum load.

Beam S1-545 was obtained when the specimens with longitudinal and transverse reinforcement with 1.0% steel fibers was tested under high torsion ($e = 0.545$ m). The horizontal strains on the concrete surface of the beam were traced by the FE model. On the one hand, the similar trends of the model and experimental data for the horizontal strain indicate increased divergence at maximum load (Fig. 27).

Increase the steel fiber ratio did not change widely the trends of FE in comparison with experimental data. Fig. 28 show a clear divergence after concrete crack for strain while a same trend shown.

The model of beams tested under low eccentricity ($e = 0.145$ m) conforms to the experimental data for horizontal strain. The model diverges and fails near the maximum load, see Fig. 29 and 30.

However, the strain analyzed in the fiber RC beams shows that the model conforms better to the fiber reinforced concrete specimens than to the plain concrete specimens. Such phenomenon is caused by the addition of steel fibers, which makes the concrete consistent and significantly prevents scattering in strain readings caused by crack control.

The strain readings are affected by several factors, such as concrete surface nature, consistency, microcracks, crack propagation, and steel reinforcing pattern. Given these factors, the data obtained from the experiment and the FE analysis are mismatched because of the difference between the concrete modeling by the SOLID65 element and the actual concrete properties.

5. Conclusions

The following conclusions are drawn based on the experimental and analytical results obtained in this study.

- The FE method can accurately predict the behavior of spandrel beams under different reinforcement and loading conditions.
- The FE model exhibits stiffness upon the collapse of the plain concrete beams.
- A smeared modeling of steel fiber RC corresponds with the experimental data.
- Softening in the FE of the RC provides superior results for beams under combined loading.

References

- ACI 318-05 (2005), American concrete institute, Building code requirements for structural concrete and commentary, Michigan.
- Adams, V. and Askenazi, A. (1998), Building Better Products with Finite Element Analysis, On Word Press, Santa Fe, New Mexico.
- ANSYS 12.0 Program, "ANSYS Manual help", Version 12, 2009.
- Avinash, S.P. and Parekar, R.S. (2010), "Steel fiber reinforced concrete beams under combined torsion-bending-shear", *J. Civil Eng.*, **38**(1), 31-38.

- Bhatti, M.A. and Almughrabi, A. (1996), "Refined model to estimate torsional strength of concrete beams", *ACI Struct. J.*, **93**(5), 614-622.
- Bangash, M.Y.H. (1989), *Concrete and Concrete Structures: Numerical Modeling and Applications*, Elsevier Science Publishers Ltd., London, England.
- Bernardo, L.F.A. and Lopes, S.M.R. (2008), "Behavior of concrete beams under torsion: NSC plain and hollow beams", *Mater. Struct.*, **41**, 1143- 1167.
- Craig, R.J., Parr, J.A., Germain, E., Mosquera, V. and Kamilaris, S. (1986), "Fiber-reinforced beams in torsion", *ACI J.*, **83**(6), 934-942.
- Dahmani, L., Khennane, A. and Kaci, S. (2010), "Crack identification in reinforced concrete beams using ANSYS software", *Strength Mater.*, **42**(2), 232-240.
- Gunneswara Rao, T.D. and Rama Seshu, D. (2003), "Torsion of steel fiber reinforced concrete members", *Cement Concrete Res.*, **33**, 1783-1788.
- Gunneswara Rao, T.D. and Rama Seshu, D. (2005), "Analytical model for the torsional response of steel fiber reinforced concrete members under pure torsion", *Cement Concrete Compos.*, **27**, 493-501.
- Hsu, T.T.C. and Mo, Y.L. (1985), "Softening of concrete in torsional members – theory and tests", *ACI J.*, **82**(3), 290-303.
- Hsu, T.T.C. and Zhang, L.X. (1997), "Nonlinear analysis of membrane elements by fixed-angle softened-truss model", *ACI Struct. J.*, **94**(5), 483-492.
- Huyse, L., Hemmaty, Y. and Vandewalle, L. (1994), "Finite Element Modeling of Fiber Reinforced Concrete Beams", Proceedings of the ANSYS Conference, Pittsburgh, Pennsylvania, May.
- Hyunjin, J.U., Deuck, H.L., Jin-Ha, H., Joo-Won, K., Kang, S.K. and Young-Hun, O. (2013), "Torsional behavior model of steel-fiber-reinforced concrete members modifying fixed-angle softened-truss model", *Compos. Part B*, **45**, 215-223.
- Kachlakev, D., Miller, T. and Yim, S. (2001), "Finite element modeling of reinforced concrete structures strengthened with frp laminates", *Oregon Dept. Transp.*, USA, Res. Group, Final Report SPR 316.
- Karayannis, C.G. (2000), "Nonlinear analysis and tests of steel-fiber concrete beams in torsion", *Struct. Eng. Mech.*, **9**(4), 323-338.
- Mahmood, N.M. (2007), "Nonlinear analysis of reinforced concrete beams under pure torsion", *J. Appl. Sci.*, **7**(22), 3524-3529.
- Mansur, M.A., Nagataki, S., Lee, S.H. and Oosumimoto, Y. (1989), "Torsional response of reinforced fibrous concrete beams", *ACI Struct. J.*, **86**(1), 36-44.
- Mansur, M.A. and Paramasivam, P. (1985), "Fiber-reinforced concrete beams in torsion, bending and shear", *ACI J.*, **82**(2), 33-39.
- Padmarajaiah, S.K. and Ramaswamy, A. (2002), "A finite element assessment of flexural strength of prestressed concrete beams with fiber reinforcement", *Cement Concrete Compos.*, **24**, 229-241.
- Parviz, S. and Lee, C. (1990), "Distribution and orientation of fibers in steel fiber reinforced concrete", *ACI Mater. J.*, **87**(5), 433-439.
- Santhakumar, R., Dhanaraj, R. and Chandrasekaran, E. (2007), "Behavior of retrofitted reinforced concrete beams under combined bending and torsion: a numerical study", *Electronic J. Struct. Eng.*, **7**(2007), 1-7.
- Swamy, R.N. and Al-ta'an, S.A. (1981), "Deformation and ultimate strength in flexure of reinforced concrete beams made with steel fiber concrete", *ACI J.*, **78**(5), 395-405.
- Thomas, J. and Ramaswamy, A. (2006), "Nonlinear analysis of shear dominant prestressed concrete beams using ANSYS", International ANSYS Conference paper. www.ANSYS.com.
- Wafa, F.F., Hasnat, A. and Tarabolsi, O.F. (1992), "Prestressed fiber-reinforced concrete beam subjected to torsion", *ACI Struct. J.*, **89**(3), 272-283.
- Wight, J.K. and Mac Gregor, J.G. (2009), *Reinforced Concrete: Mechanics and Design*, Pearson Prentice Hall, New Jersey, USA.